# RESEARCH ON THE PROPERTIES OF THE ARMCHAIR SISN NANORIBBONS APPLIED IN NANOELECTRONICS AND OPTOELECTRONICS

**Tran Minh Tien**[(1)]
*(1) Thu Dau Mot University*
*Corresponding author: tientm@tdmu.edu.vn*

**DOI: 10.37550/tdmu.EJS/2025.01.616**

## Article Info

**Volume:** 7
**Issue:** 1
**March:** 2025
**Received:** Dec. 8th, 2024
**Accepted:** Jan. 20th, 2025
**Page No:** 114-123

## Abstract

The paper presents the results of a study on the essential physical properties of armchair SiSn nanoribbon (SiSnNR) material, based on density functional theory (DFT) using the quantum simulation program VASP. Structural parameters are highlighted along with electronic and optical properties. The findings reveal that SiSnNR exhibits significant differences in bond lengths, bond angles, and buckling compared to SiNR and SnNR. SiSnNR demonstrates semiconducting properties, with a direct band gap width of approximately 0.3123Å calculated using GGA-PBE, increasing to 0.5892Å when using the hybrid HSE06 functional. The results indicate that Sn atoms primarily contribute to energy bands below the Fermi level, while Si atoms contribute more to higher energy levels. The study also highlights the overlap of py and pz orbitals, leading to sp2 and sp3 hybridization. In terms of optical properties, the energy range from 3 to 5eV is where SiSnNR exhibits the strongest light absorption. The largest number of electron-hole pairs is generated within the energy range of 8-10eV, resulting in intense optical absorption and transitions in this region.

**Keywords:** armchair SiSn nanoribbon, electronic properties, optical properties, VASP

## 1. Introduction

Nanoribbon materials have garnered significant research interest due to their immense potential applications in optoelectronics, nanoelectronics, and sensing. Several prominent nanoribbon systems include graphene nanoribbons, silicene nanoribbons, phosphorene nanoribbons, and stannene nanoribbons. Since 2009, nanoribbons have been developed on silver surfaces using the chemical vapor deposition (CVD) method (Le Lay et al., 2009). Studies utilizing scanning tunneling microscopy (STM), X-ray photoelectron spectroscopy (XPS), and density functional theory (DFT) revealed that silicene nanoribbons with a width of approximately 1.6nm are aligned parallel on silver surfaces, exhibiting unique electronic properties with quantized electronic states and strong metallicity. In 2012, the thermoelectric properties of armchair and zigzag silicene nanoribbons were studied in detail (Pan et al., 2012) using the non-equilibrium Green's

function (NEGF) method combined with non-equilibrium molecular dynamics (NEMD) simulations. Structural optimization and electronic properties of SiNRs were calculated using DFT, with the Vienna Ab Initio Simulation Package (VASP) and Atomistix Toolkit (ATK) employed for electronic transport coefficients. The results indicated that SiNRs are structurally stable when edge atoms are passivated with hydrogen. Armchair-edged SiNRs generally exhibit better thermoelectric performance than zigzag-edged SiNRs. Thermoelectric effects in silicene nanoribbons were further investigated in detail by Zberecki and colleagues (Zberecki et al., 2013). The study, based on DFT and the NEGF method, calculated transport and thermoelectric coefficients. Results showed that zigzag silicene nanoribbons exhibit edge magnetism with antiferromagnetic and ferromagnetic configurations. The Seebeck coefficient strongly depends on the electronic band structure and is enhanced when the Fermi level lies within the energy gap. However, thermoelectric performance decreases significantly when phonon contributions to thermal conductivity are included. In 2014, a study evaluating the potential of silicene nanoribbons for detecting CO gas molecules was conducted (Tim Osborn et al., 2014). The results indicated that CO weakly adsorbs onto silicene nanoribbons, causing charge transfer from CO to silicene and structural deformation. These findings confirm the potential of silicene nanoribbons in gas sensing applications. Spin and charge transport properties in zigzag silicene nanoribbons under external electromagnetic fields were also explored (Shakouri et al., 2015). The study showed that the structure of zigzag silicene nanoribbons lacks spin-reversal symmetry when intrinsic spin-orbit interactions and external electromagnetic fields are combined, enabling high-performance tunable spin polarizers. Additionally, the combination of external electromagnetic and exchange fields can produce nearly perfect spin polarization. This research highlights that tuning external electromagnetic fields can enhance the spin transport properties of silicene nanoribbons.

The properties of nanoribbon materials with hybrid structures composed of Si and C, or other types of atoms, have also been investigated. In 2008, the electronic structural properties of SiC nanoribbons were reported (Lian Sun et al., 2008; Ping Lou et al., 2009; Jian-Min Zhang et al., 2010). The results indicated that SiC nanoribbons exhibit semiconductor or metallic properties depending on their edge structure and width. Narrow zigzag-edged SiC nanoribbons less than 0.6nm wide are nonmagnetic semiconductors with a large band gap. Zigzag-edged SiC nanoribbons wider than 0.6nm exhibit ferrimagnetic semiconductor properties with two distinct direct band gaps for spin-up and spin-down states. Zigzag-edged SiC nanoribbons generally exhibit metallic properties, except for very narrow ribbons (Nz = 2–4) that display a small band gap. Armchair-edged SiC nanoribbons are semiconductors with oscillating band gaps that stabilize to a constant value as the width increases. The electronic band structure and optical properties of SiC nanoribbons have also been studied (Naresh Alaal et al., 2016; Hojat Allah Badehian et al., 2021). Results revealed significant quasiparticle corrections in SiC nanoribbons, with quasiparticle band gaps increasing by up to 2eV compared to Kohn-Sham energy values. Electron-hole interactions significantly altered the absorption spectra, producing strong excitonic peaks in these systems.

Stanene nanoribbons have also been a subject of extensive research. The structural, electronic, thermal, and optical properties have been studied (Wenqi Xiong et al., 2016; Asir Intisar Khan et al., 2017; Jingshan Qi et al., 2018; Fadaie et al., 2018). The results indicate that the electronic properties of armchair stanene nanoribbons (ASnRs) strongly depend on their width, with band gaps ranging from a few meV to approximately 0.4-0.5eV.

Anisotropy in the optical properties of ASnRs is observed under different light polarizations. Zigzag stanene nanoribbons consistently exhibit insulating properties, with band gaps dependent on the magnetization direction and the magnetic coupling between the edges.

The results show that SiNR and SnNR possess high potential for applications in various fields, such as optoelectronic technology, spintronic devices, and quantum spin Hall effect systems. Nano materials doped with a combination of Si and Sn also hold significant application potential but have not yet been comprehensively and thoroughly studied in detail. In this paper, the structural, electronic, and optical properties of these materials are investigated in detail to evaluate their potential and provide guidance for their future applications. The structure of the armchair SiSnNR is studied, and the zigzag SiSnNR will be studied in the next works.

## 2. Research models and methods

The unit cell of ASiSnNR was composed of six Si atoms, six Sn atoms, and four functional H atoms at the side edges to enhance the stability of the structure. The dimensions of the a, b, and c axes of the unit cell are set at 20.0Å, 25.5Å and 8.48Å, respectively; to ensure the circularity of the structure when creating a super cell. To study the electronic and optical properties of the structures, density functional theory (DFT) calculations were employed using the Vienna Ab initio Simulation Package (VASP) (Kresse et al., 1996 ). The exchange-correlation energies of electrons were computed based on the generalized gradient approximation (GGA) (Perdew et al., 1996), utilizing the Perdew–Burke–Ernzerhof (PBE) functional and the Projector-Augmented Wave (PAW) method (Kresse et al., 1999). To further clarify the PBE calculation results, the electronic band structure was also computed using the Heyd-Scuseria-Ernzerhof (HSE06) hybrid functional (Heyd et al., 2003). The wave functions and energy states were constructed from a plane-wave basis set with a maximum energy cutoff of 350eV. The k-point grids in the Monkhorst-Pack scheme used for structural optimization calculations were 1×1×8. The system was optimized until the forces were less than EDIFFG = $-10^{-8}$ eV/Å, as per the Hellmann–Feynman force limit. The energy convergence was set to EDIFF = $10^{-8}$ eV between consecutive ionic steps. The optimized unit cell structure of the system is shown in Figure 1. Self-consistent calculations were performed after structural optimization. The electronic band structure, density of states (DOS), charge density distribution, spin density distribution, and optical properties were subsequently investigated. The optical properties of the structure are investigated through the dielectric function. Many other optical properties, such as the absorption coefficient and the reflectivity coefficient, are derived from the dielectric function.

## 3. Results and discussion

### *3.1. Optimal post-structure*

The optimized structure of SiSnNR is shown in Figure 1, and its structural parameters are listed in Table 1. The fundamental parameters include the bond lengths between two neighboring Si-Sn atoms, the bond angles in the hexagonal rings, and the buckling height. Table 1 also presents the parameters for the SiNR and SnNR structures for comparison, highlighting the changes in structural parameters resulting from the doping configuration.

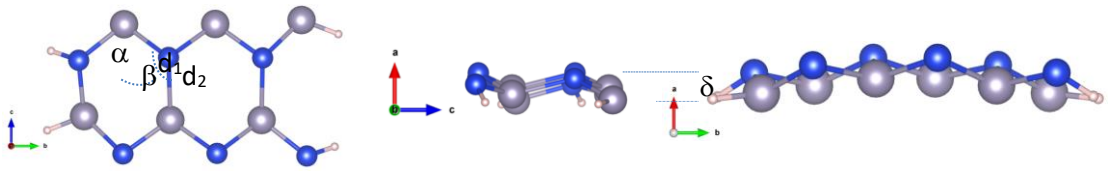


(a) (b) (c)

***Figure 1***. The structure of SiSnNR

The results show that SiSnNR exhibits significant differences in bond lengths, bond angles, and buckling compared to SiNR and SnNR. These differences may influence the electronic and mechanical properties of the nanoribbon. The Si-Sn bond length in SiSnNR is larger than the Si-Si bond length in SiNR but smaller than or approximately equal to the Sn-Sn bond length in SnNR, reflecting an intermediate atomic size balance between Si and Sn. The buckling in SiSnNR is considerably higher than in both SiNR and SnNR, likely due to the difference in atomic radii between Si and Sn, causing uneven stress in the structure. Consequently, the bond distances (d1 and d2) in SiSnNR are intermediate between those of SiNR and SnNR, with d2 tending to be larger due to the influence of Sn atoms. The α angle decreases, while the β angle increases, indicating significant structural distortion in SiSnNR. The increased buckling (δ) in SiSnNR could have a substantial impact on the electronic and mechanical properties of the material system.

*TABLE 1*. The structural parameters of SiSnNR

| Configuration | d1 (Å) | d2 (Å) | α (Å) | β (Å) | δ (Å) |
|---|---|---|---|---|---|
| SiNR | 2.25 | 2.25 | 108.05 | 108.05 | 0.80 |
| SnNR | 2.77 | 2.82 | 109.00 | 111.04 | 0.86 |
| SiSnNR | 2.63 | 2.85 | 100.61 | 118.70 | 1.16 |

### *3.2. Electronic band structure and density of states*

The analysis of the electronic band structure and density of states (DOS) reveals the fundamental electronic properties of the material system. The results indicate a direct bandgap of approximately 0.3123eV as calculated using GGA-PBE, and up to 0.5892eV with the hybrid functional HSE06. This demonstrates that SiSnNR exhibits the characteristics of a semiconductor with a relatively large bandgap, suggesting its high potential for applications in nanoelectronics.

Figure 2 illustrates the electronic band structure of the SiSnNR system in detail. Specifically, Figure 2(a): Shows the contributions from all atoms; Figure 2(b): depicts the individual contributions of Si and Sn atoms, Figures 2(c) and 2(d): Highlight the contributions of the s, py, pz, and px orbitals for each atom. The results reveal that Sn atoms predominantly contribute to energy bands below the Fermi level, while Si atoms contribute more to bands above the Fermi level. This suggests that Sn atoms play a major role in electronic states near the Fermi level, significantly influencing the conductive properties. The pz orbital of Si notably contributes to energy levels near the Fermi level, particularly in the conduction band, while the px and py orbitals contribute more to energy bands further below and above the Fermi level. This underscores the importance of the Si pz orbital in conduction. Similarly, the pz orbital of Sn is dominant near the Fermi level, but the px and py orbitals of Sn exhibit a broader energy distribution compared to Si. Additionally, the s orbital of Sn makes significant contributions at lower energy levels, reflecting its involvement in valence electronic states.

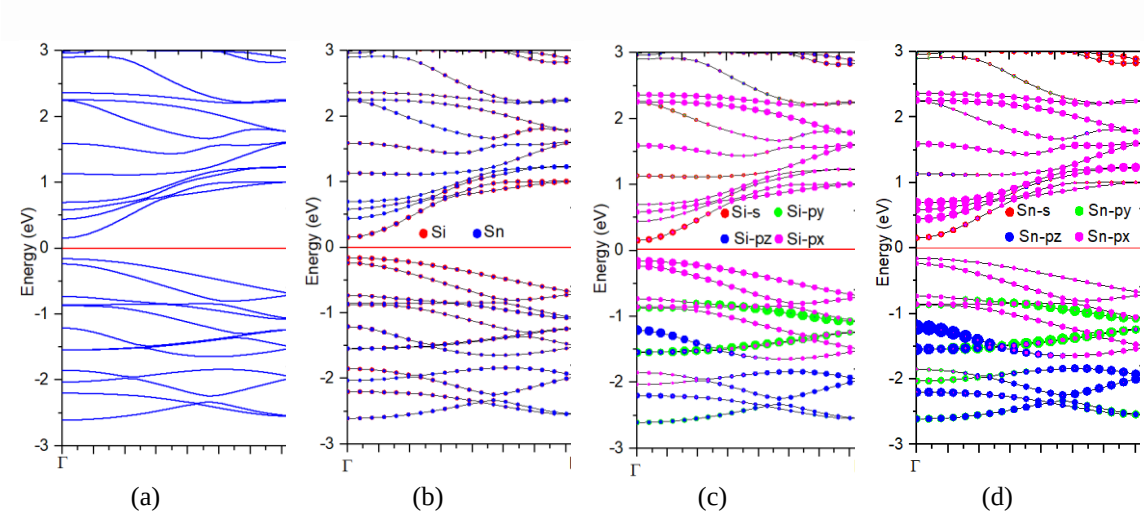


***Figure 2***. The electronic band structure of the SiSnNR

Figure 3 presents the distribution of the electronic density of states (DOS); figure 3(a) displays the total DOS and contributions from Si and Sn atoms; figures 3(a) and 3(b): illustrate the DOS distribution corresponding to the s, px, py, and pz orbitals of each Si and Sn atom. The results reveal that the DOS peaks are concentrated in two regions: around the Fermi level and within the energy range of -2 to -3 eV. Sn atoms dominate in the lower energy region, while Si atoms primarily contribute to the higher energy region. Orbital contributions show that the Si-pz orbital has a prominent peak near the Fermi level, consistent with the results from Figure 2(c), confirming its primary role in electrical conduction. In contrast, the Si-px and Si-py orbitals exhibit a broader DOS distribution with smaller peaks at energy levels further from the Fermi level. The Si-s orbital contributes minimally to electronic states near the Fermi level and is mainly concentrated at lower energy levels. Similarly, the Sn-pz orbital exhibits the largest contribution near the Fermi level, mirroring the behavior of Si. The Sn-px and Sn-py orbitals show lower DOS but a broader energy distribution compared to Si, while the Sn-s orbital forms significant peaks in the low-energy range (-2 eV to -3 eV), indicating a strong involvement in valence electronic states.

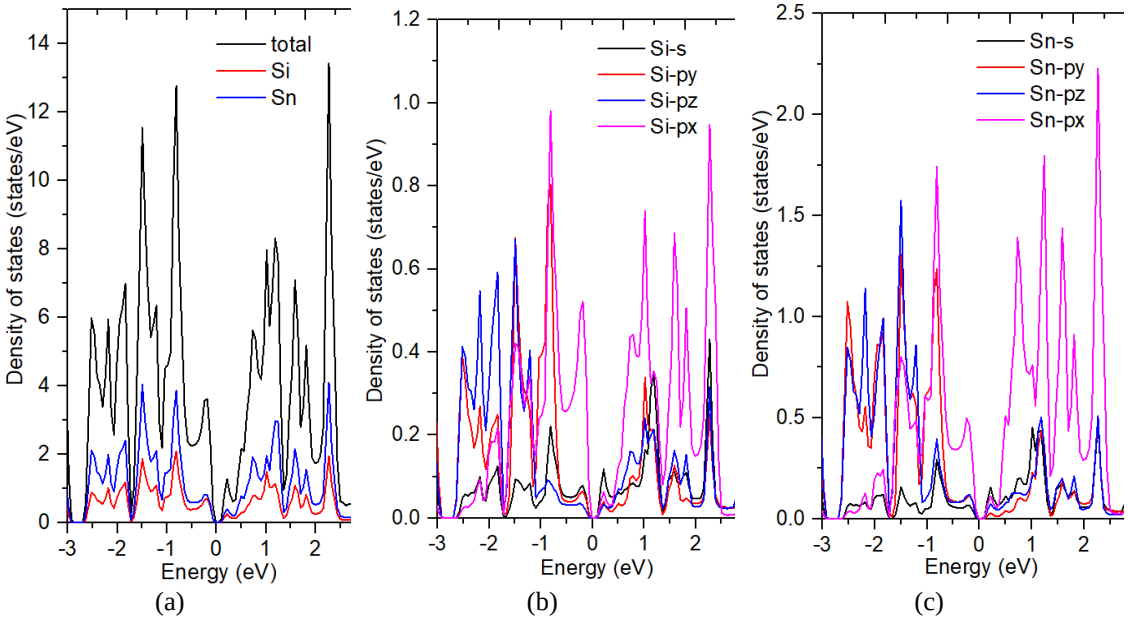


***Figure 3.*** The density of states of SiSnNR

Thus, the analysis of the electronic band structure and density of states distribution shows that SiSnNR exhibits semiconductor properties, with Sn contributing more to the valence states, while Si primarily contributes to the conduction band (higher energy region above the Fermi level). The pz orbitals of both Si and Sn play a dominant role in electrical conduction. The peaks in the density of states near the Fermi level confirm that the material has high electrical conductivity, primarily influenced by the pz orbitals of both Si and Sn. The results also indicate the overlap of the py and pz orbitals, leading to $sp^2$ and $sp^3$ hybridization. Si tends to favor $sp^2$ hybridization, facilitating the formation of a π-bonded network that conducts electricity well. Sn, on the other hand, tends toward $sp^3$ hybridization, influenced by significant buckling and notable contributions from the px, py, and s orbitals in σ bonds. The combination of $sp^2$ and $sp^3$ hybridization contributes to the unique electrical and mechanical properties of SiSnNR.

### *3.3. Charge density distribution*

Figure 4 presents the charge density distribution of the SiSnNR structure. Figure 4(a) shows the 3D charge density distribution, Figure 4(b) illustrates the 2D cross-sectional charge density, and Figure 4(c) indicates the local bonding between two Si and Sn atoms. The results show high charge density around the bonds, with an asymmetric distribution between the Si and Sn atoms reflecting the difference in their electronegativity. The Sn atom, with a lower electronegativity, attracts less charge, resulting in a lower charge density region, while the Si atom, with a higher electronegativity, attracts more charge, creating a higher charge density region. The concentration of charge density between the Si and Sn atoms indicates the strong covalent nature of the bond. The bond polarization enhances electronic interactions, affecting the electrical and optical properties of SiSnNR. Stronger polarization occurs at the Si-Sn bonds, especially when considering the charge density along the pz orbitals (as analyzed in Figures 2 and 3).

This charge density distribution plays a crucial role in the electrical conductivity and semimetallic properties of SiSnNR. The regions of high charge density around Si and Sn affect surface chemical reactions, enhancing the material's ability to interact with other substances, which is beneficial for sensor or catalysis applications.

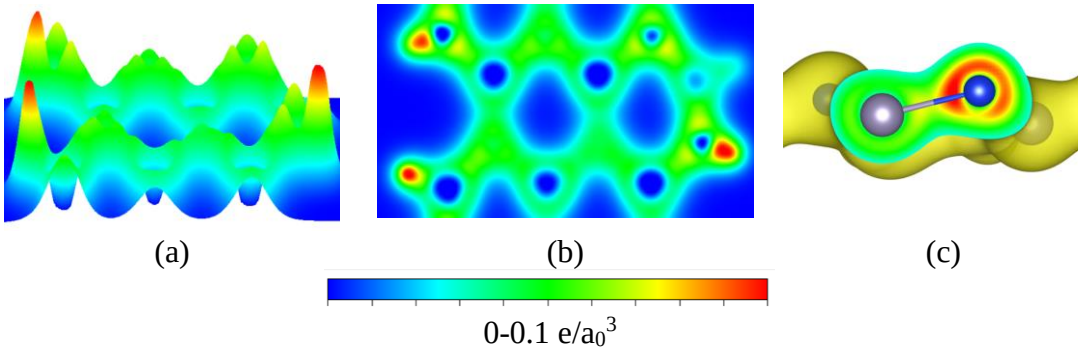


***Figure 4.*** The charge density distribution of the SiSnNR

### *3.4. Real space wave function in VBM and CBM*

The investigation of wavefunction distribution at the Valence Band Maximum (VBM) and Conduction Band Minimum (CBM) of SiSnNR further elucidates its electronic properties, bonding structure, and hybridization. Figure 5 illustrates the wavefunction distribution, with Figures 5(a), 5(b), 5(c) depicting the VBM region and Figures 5(d), 5(e), 5(f) representing the CBM region. The wavefunction at the VBM is primarily

localized around Sn atoms, indicating that covalent bonding electrons near the VBM are predominantly influenced by Sn due to its larger atomic radius and lower electronegativity compared to Si. The states near the VBM are likely governed by the p orbitals of Sn, mainly pz or px/py, with the wavefunction concentrated along Si-Sn bonds, suggesting strong covalent bonding and $sp^2$ hybridization within the bonding plane. In contrast, the CBM wavefunction is primarily localized around Si atoms, showing that conduction states at the CBM are mainly controlled by Si due to the higher mobility of electrons in this region. These states are likely derived from s or p orbitals of Si, with px/py playing a significant role. The symmetric distribution of wavefunctions at the CBM reveals antibonding characteristics, with notable contributions from the pz orbitals of both Si and Sn, further suggesting $sp^2$ or $sp^3$ hybridization in the Si-Sn bonds. The electrons at the CBM are more delocalized across the crystal lattice, enhancing the electrical conductivity of SiSnNR. Overall, these results highlight the dominant role of Sn near the VBM and Si near the CBM, with the pz orbitals of both elements being crucial for electrical conduction.

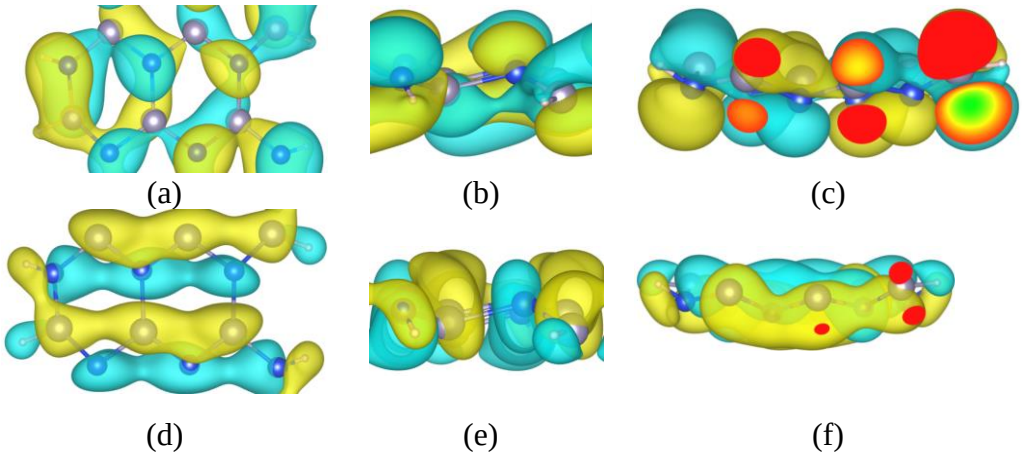


***Figure 5.*** The Real space wave function in VBM and CBM

The CBM wavefunction is widely distributed and delocalized, indicating good electrical conductivity when the material is excited. This aligns with the semiconducting nature of SiSnNR, showcasing its potential for applications in electronic and optical devices. The distinct wavefunction distribution at the VBM and CBM (nearly direct bandgap) suggests that the material can efficiently absorb and emit light, making it suitable for optical applications. The VBM and CBM structure, combined with the appropriate bandgap, underscores the material's suitability for use in semiconductor devices, particularly in optoelectronic technology and sensors.

### *3.5. Optical properties*

The absorption and reflection characteristics are also crucial properties to investigate. Figures 6(a) and 6(b) present the absorption and reflection spectra of SiSnNR as a function of incident photon energy, while Figures 6(c) and 6(d) illustrate the real and imaginary components of the dielectric function, respectively. Additionally, Figure 6(e) shows the optical joint density of states (JDOS).

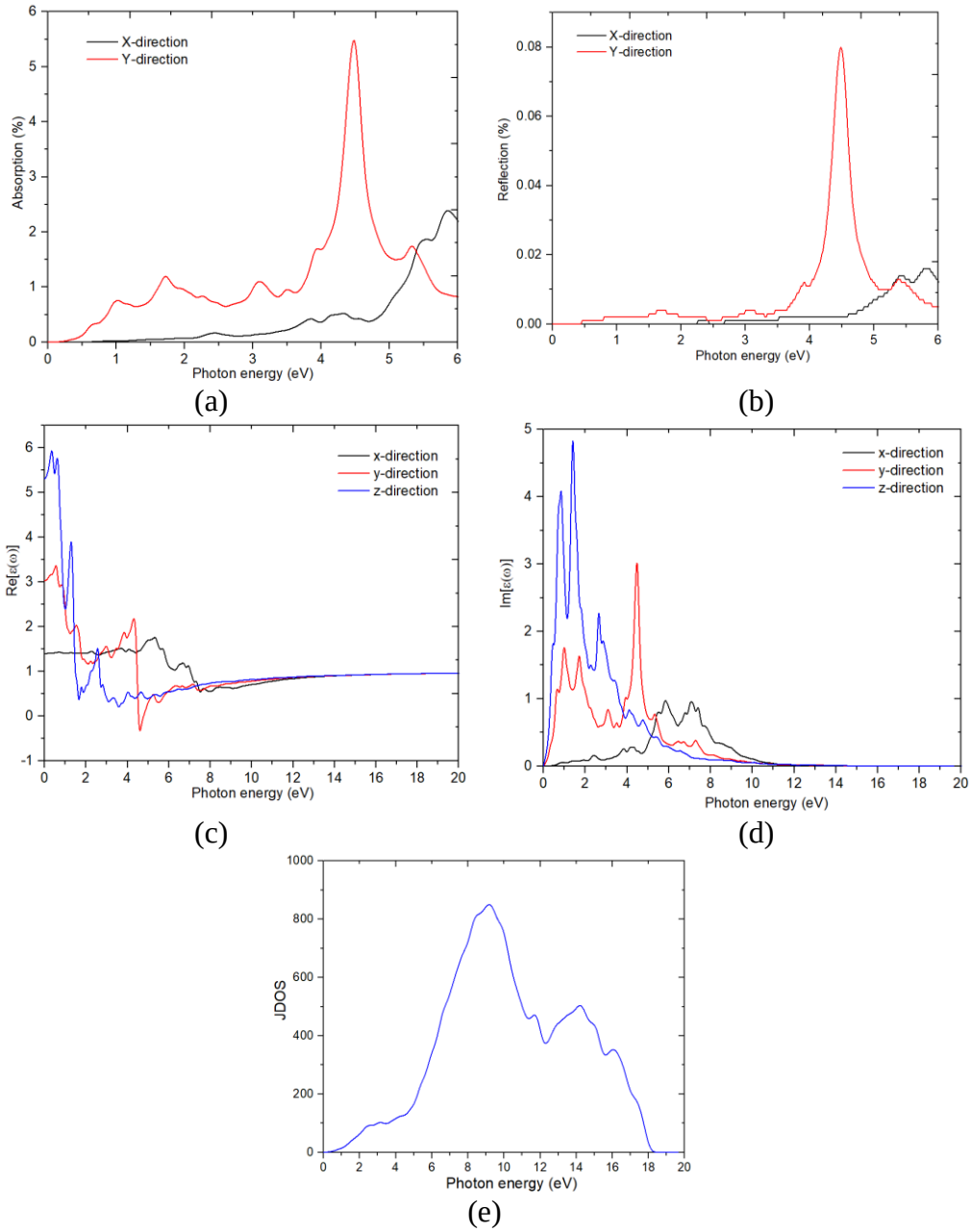


***Figure 6.*** The absorption and reflection spectra of SiSnNR as a function of incident photon energy (a,b); the real and imaginary components of the dielectric function (c,d); the optical joint density of states (e)

The absorption spectra indicate that SiSnNR exhibits strong light absorption in the energy range of 3-5eV, making it suitable for applications in the near-ultraviolet (UV) region. Anisotropy is evident from the significant differences between the X and Y directions, suggesting that the optical properties of SiSnNR are strongly dependent on the crystal orientation. This could be attributed to the varying orbital distributions of Si and Sn atoms along different directions.

The reflection spectra reveal a low reflection coefficient, indicating that SiSnNR allows light to pass through efficiently, which is advantageous for optical applications requiring reduced reflectivity, such as solar cells or sensors. The real part of the dielectric function,

Re(ε), peaks around 4-5eV and gradually decreases at higher energies. The high Re(ε) value in the UV range suggests that the material can effectively store electromagnetic energy in this region, making it suitable for photonic devices or sensors. The imaginary part of the dielectric function, Im(ε), reaches a maximum around 4.5eV and a secondary peak at 5.5eV, corresponding to electronic transitions from the valence band (VB) to the conduction band (CB). The peaks in Im(ε) identify specific energy ranges where the material interacts strongly with light, highlighting its potential for designing light-emitting or light-absorbing devices.

The JDOS analysis shows the highest electron-hole pair generation in the energy range of 8-10 eV, leading to strong optical absorption and transition processes in this region. The low JDOS in the low-energy range (<2eV) reflects the bandgap of SiSnNR, consistent with its semiconducting nature.

## 4. Conclusion

A nanoribbon structure doped with Si and Sn has been constructed and optimized for atomic positions. Structural differences between SiSnNR and pristine Si or Sn nanoribbons, including bond lengths, bond angles, and buckling have been indicated. Electronic characteristics such as electron band structure, band gap, density of state, and charge density distribution are indicated. The large bandgap of SiSnNR offers significant potential for applications in nanoelectronics. Optical characteristics such as absorption coefficient, light emission, real part, and dielectric function phantom part are also presented. Optical properties demonstrate that SiSnNR exhibits a wide optical absorption range and anisotropy; its absorption spectra, reflectivity, and dielectric function show marked differences between the X and Y directions, reflecting the asymmetric structure of the material. The low reflectivity of SiSnNR enables efficient light transmission, making it promising for applications such as anti-reflective coatings or solar energy absorbers. The material interacts strongly with light in the 8-10eV energy range, indicating suitability for photonic applications. With these properties, SiSnNR is a strong candidate for use in optical sensors, anti-reflective coatings, UV light-emitting devices, and high-efficiency solar energy devices.

***Acknowledgement***

*This research used resources of the high-performance computer cluster (HPCC) at Thu Dau Mot University*

## References

Alaal, N., Loganathan, V., Medhekar, N., & Shukla, A. (2016). First principles many-body calculations of electronic structure and optical properties of SiC nanoribbons. *Journal of Physics D: Applied Physics*, *49*(10), 105306.

Badehian, H. A., Badehian, Z., & Sharifirad, R. (2021). Structural and Electronic Properties of Armchair Silicon Carbide Nanoribbon. *Current Applied Sciences*, *1*(1), 51-58.

Fadaie, M., Shahtahmassebi, N., Roknabad, M. R., & Gulseren, O. (2018). First-principles investigation of armchair stanene nanoribbons. *Physics Letters A*, *382*(4), 180-185.

G. Kresse and D. Joubert (1999), From ultrasoft pseudopotentials to the projector augmented-wave method. *Phys. Rev. B*, 59.

G. Kresse and J. Furthmüller (1996). Efficiency of ab-initio total energy calculations for metals and semiconductors using a plane-wave basis set. *Comput. Mater. Sci*, 6, 1.

G. Kresse and J. Furthmüller (1996). Efficient iterative schemes for ab initio total-energy calculations using a plane-wave basis set. *Phys. Rev. B*, 54, 16.

Heyd, J.; Scuseria, G.E.; Ernzerhof, M. (2003. Hybrid functionals based on a screened Coulomb potential. *J. Chem. Phys*, 118, 8207-8215

J. P. Perdew, K. Burke, and M. Ernzerhof (1996). Generalized gradient approximation made simple. *Phys. Rev. Lett*, 77, 18.

Khan, A. I., Paul, R., & Subrina, S. (2017). Characterization of thermal and mechanical properties of stanene nanoribbons: a molecular dynamics study. *RSC advances*, *7*(80), 50485-50495.

Le Lay, G., Aufray, B., Léandri, C., Oughaddou, H., Biberian, J. P., De Padova, P., ... & Kara, A. (2009). Physics and chemistry of silicene nano-ribbons. *Applied Surface Science*, *256*(2), 524-529.

Lou, P., & Lee, J. Y. (2009). Band structures of narrow zigzag silicon carbon nanoribbons. *The Journal of Physical Chemistry C*, *113*(29), 12637-12640.

Osborn, T. H., & Farajian, A. A. (2014). Silicene nanoribbons as carbon monoxide nanosensors with molecular resolution. *Nano Research*, *7*, 945-952.

Pan, L., Liu, H. J., Tan, X. J., Lv, H. Y., Shi, J., Tang, X. F., & Zheng, G. (2012). Thermoelectric properties of armchair and zigzag silicene nanoribbons. *Physical Chemistry Chemical Physics*, *14*(39), 13588-13593.

Qi, J., Hu, K., & Li, X. (2017). Electric control of the edge magnetization in zigzag stanene nanoribbon. *arXiv preprint arXiv:1706.09098*.

Shakouri, K., Simchi, H., Esmaeilzadeh, M., Mazidabadi, H., & Peeters, F. M. (2015). Tunable spin and charge transport in silicene nanoribbons. *Physical Review B*, *92*(3), 035413.

Sun, L., Li, Y., Li, Z., Li, Q., Zhou, Z., Chen, Z., ... & Hou, J. G. (2008). Electronic structures of SiC nanoribbons. *The Journal of chemical physics*, *129*(17).

Xiong, W., Xia, C., Peng, Y., Du, J., Wang, T., Zhang, J., & Jia, Y. (2016). Spin–orbit coupling effects on electronic structures in stanene nanoribbons. *Physical Chemistry Chemical Physics*, *18*(9), 6534-6540.

Zberecki, K., Wierzbicki, M., Barnaś, J., & Swirkowicz, R. (2013). Thermoelectric effects in silicene nanoribbons. *Physical Review B—Condensed Matter and Materials Physics*, *88*(11), 115404.